critical strains show that the dislocation stops before it starts to move again subsonically.

The observed transition to the supersonic state and the greater increase of dislocation velocity in the supersonic regime cannot be understood from the linear elastic analysis because $A(v)$ monotonically increases with the velocity of the dislocation above $\sqrt{2}c_T$ (Fig. 4). The second sound barrier at c_L therefore must be entirely caused by the nonlinearity and the finite range of the atomic interaction in the dislocation core region. This is displayed by the asymmetry of the longitudinal shock waves emanating from the supersonic dislocation (Fig. 3D). Linear elasticity would predict one symmetrical pair of shock fronts, whereas the atomistic simulations show a much richer distribution. The upper, compressive part of the dislocation produces a series of very severe shock fronts, whereas the lower side develops only one front. Whether this asymmetry has its origin in the sign of the stress field of the dislocation or whether it is a result of crystal orientation cannot be decided from the present calculations alone.

Comparing the atomistic simulations in a finite thin strip with continuum elasticity theory for an infinite sample and attributing some of the observed features to nonlinearities is of course questionable as long as one has not investigated size effects in the atomistic model. To do so, we repeated the calculations for a model in which all lengths were changed by a factor of 2 for the case of an externally applied strain of $\varepsilon = 0.05$. Whereas the smaller system gives a 10% slower dislocation, the large system is almost indistinguishable from the system used so far in both the dislocation velocity and the distribution of the atomic velocities around the dislocation core (compare Fig. 3C). Although these results, of course, do not constitute a proper system-size scaling analysis, they give confidence that the conclusions drawn so far are not critically dependent on system size.

The practical importance of these transonic and supersonic dislocations appears to be limited by the difficulty of nucleation and by the high stresses that are required for sustained motion at these high velocities. From the discussion of the nucleation conditions, it has been concluded that an intense stress concentration is required for the nucleation of transonic dislocations. Stress concentrators with an efficiency similar to that of the sharp indenter could either be a dislocation pileup at a strong obstacle or a crack, which is characterized by a stress singularity at its tip. Conditions that give the extremely high background stresses required for continuous long-distance propagation at the transonic or supersonic speed are present in low-temperature deformation, where thermally activated deformation processes are suppressed. In addition to the motion of individual dislocations, deformation at low temperatures is often carried by mechanical twinning, which can be viewed as the concerted motion of several partial (twinning) dislocations. Consequently, one may also regard low-temperature mechanical twinning as a case where transonic motion could be observable. The motion of mechanical twins above c_T has indeed been predicted for applied stresses (or strains) above a critical value in an analytical nonlinear elasticity study (*14*). Using high-speed photography, Finkel' (*15*) has documented that the first thin twins formed in dynamically loaded steel sheets propagate at velocities of $0.80c_L$ to $0.85c_L$, corresponding almost exactly to the transonic velocity regime observed here. In later stages of the deformation, twins were observed to move at velocities of $0.40c_L$ to $0.45c_L$, corresponding to the subsonic regime in Fig. 2.

Whether supersonic dislocations may be relevant for geophysical phenomena is as yet unclear. On the one hand, the increasing temperature in the deeper crust makes thermally activated processes more likely; on the other hand, low-symmetry crystal structures and the limited amount of slip systems certainly allow the buildup of large stresses, which may reach the required order of magnitude.

Future work should focus on the nucleation conditions that result in supersonic dislocations. Supersonic dislocations may help to understand some of the deformation phenomena that are usually considered collective, and therefore, the dynamics of mechanical twinning, martensitic transformation, and tectonic shear faults may have to be reinvestigated while considering the results presented here.

References and Notes

1. J. P. Hirth and J. Lothe, *Theory of Dislocations* (Wiley, New York, 1982).
2. J. D. Eshelby, *Proc. R. Soc. London A* **62**, 307 (1949).
3. J. Weertman, in *Mathematical Theory of Dislocations*, T. Mura, Ed. (American Society of Mechanical Engineers, New York, 1969), pp. 178–202.
4. F. R. N. Nabarro, *Theory of Crystal Dislocations* (Oxford Univ. Press, Oxford, 1967).
5. J. Weertman and J. R. Weertman, in *Dislocations in Solids*, F. R. N. Nabarro, Ed. (North-Holland, Amsterdam, 1980), vol. 3, pp. 1–60.
6. H. Gao, Y. Huang, P. Gumbsch, A. J. Rosakis, *J. Mech. Phys. Solids*, in press.
7. A. J. Rosakis, D. Coker, O. Samundrala, *Caltech SM Rep. 98-17* (California Institute of Technology, Pasadena, 1998).
8. R. J. Archuletta, *Bull. Seismol. Soc. Am.* **72**, 1927 (1982).
9. J. Schiotz, K. W. Jacobsen, O. H. Nielsen, *Philos. Mag. Lett.* **72**, 245 (1995).
10. P. Gumbsch, *Z. Metallkd.* **87**, 341 (1996).
11. M. W. Finnis and J. E. Sinclair, *Philos. Mag. A* **50**, 45 (1984).
12. G. J. Ackland and R. Thetford, *ibid.* **56**, 15 (1987).
13. J. Friedel, *Dislocations* (Pergamon, Oxford, 1964).
14. P. Rosakis and H. Tsai, *Int. J. Solids Struct.* **32**, 2711 (1995).
15. V. M. Finkel', I. N. Voronov, A. M. Savel'Yev, A. I. Yeliseyenko, V. A. Fedorov, *Fiz. Met. Metalloved.* **29**, 1248 (1970).

16. Inspiring discussions with R. Phillips, Brown University, on the nucleation of supersonic dislocations as well as his suggestion of the indenter geometry are gratefully acknowledged. H.G. would like to thank the Alexander von Humboldt foundation for financial support of his stay at the Max-Planck-Institut für Metallforschung in Stuttgart.

21 September 1998; accepted 6 January 1999

Chemical Analysis of Polar Stratospheric Cloud Particles

Jochen Schreiner,[1] Christiane Voigt,[1] Andreas Kohlmann,[1] Frank Arnold,[1] Konrad Mauersberger,[1]* Niels Larsen[2]

A balloon-borne gondola carrying a particle analysis system, a backscatter sonde, and pressure and temperature sensors was launched from Kiruna, Sweden, on 25 January 1998. Measurements within polar stratospheric cloud layers inside the Arctic polar vortex show a close correlation between large backscatter ratios and enhanced particle-related water and nitric acid signals at low temperatures. Periodic structures in the data indicate the presence of lee waves. The H_2O/HNO_3 molar ratios are consistently found to be above 10 at atmospheric temperatures between 189 and 192 kelvin. Such high ratios indicate ternary solution particles of H_2O, HNO_3, and H_2SO_4 rather than the presence of solid hydrates.

The important role of polar stratospheric clouds (PSCs) during the development of the south polar ozone hole was recognized soon after the first publication (*1*) on large unexpected ozone losses in the lower stratosphere over Antarctica. Initially, the existence of cloud particles at temperatures above the ice point was puzzling; however, thermodynamic considerations (*2*) as well as laboratory studies (*3*) revealed that in the H_2O-HNO_3 system stable crystalline hydrates can be formed above the ice point. During the last 10 years the initial concept of two types of PSCs—

[1]Max-Planck-Institut für Kernphysik, Division of Atmospheric Physics, Post Office Box 103 980, D-69029 Heidelberg, Germany. [2]Danish Meteorological Institute, Division of Middle Atmosphere Research, Lyngbyvej 100, DK-2100 Copenhagen, Denmark.

*To whom correspondence should be addressed.

nitric acid trihydrate (NAT, $HNO_3 \cdot 3H_2O$) and ice particles (*4*)—has been expanded to explain Lidar and backscatter sonde measurements. Supercooled ternary solutions or amorphous particles composed of nitric acid, water, and sulfuric acid may frequently be present in a temperature range in which solid NAT particles are thermodynamically stable (*5*). Laboratory studies and model developments of heterogeneous processes have advanced to the point that the phase and the composition of PSC particles as a function of ambient temperatures, gas-phase HNO_3, and water vapor abundances can be predicted (*6*); however, a detailed chemical analysis of PSC particle composition has never been made (*7*). The particles exist over a very narrow temperature range (*8*), and thus the transfer to or capture into an analytical instrument may easily alter their phase and composition.

A PSC analysis instrument has been developed in our laboratory that circumvents most of the potential shortcomings in the transfer of the fragile particles from ambient air into a mass spectrometer system. The instrument consists of an aerodynamic lens that focuses PSC particles into a narrow beam (*9*, *10*), a differentially pumped vacuum system containing two liquid helium pumps, a small particle evaporation sphere, and a quadrupole mass spectrometer for gas analysis (Fig. 1). The main goal of the experiment was a quantitative analysis of condensed water and nitric acid contained in PSC particles (*11*).

The lens is thermally isolated to remain near ambient temperatures during the balloon flight. Particles traverse the lens in about 50 ms and reach the evaporation sphere in less than 0.5 ms after acceleration at the exit hole of the lens (*10*, *12*). Because of these rapid transfers, little or no evaporation or condensation should take place from the ambient atmosphere into the evaporation sphere.

Until the later part of January 1998, lower stratospheric temperatures above Kiruna, Sweden, were too high for PSC activity to occur. After January 20 a cooling trend started and lee wave–induced PSC activity was predicted across the Scandinavian mountains (*13*). The balloon was launched on 25 January 1998 at 0:30 UT from the Swedish launch facility ESRANGE near Kiruna. A backscatter sonde (*14*) and temperature (*15*) and pressure sensors were also part of the balloon payload. Using the backscatter sonde signals to identify the presence of PSC layers, the balloon operators were able to raise or lower the balloon and gondola by opening a valve or dropping ballast to keep the experiment within the altitude range of 20 to 23.5 km. Mass spectrometer measurements were performed between 2:00 and 4:00 UT during which time the balloon was located inside the Arctic polar vortex.

Trajectory calculations of the air masses encountered by the balloon show a large-scale cooling from nearly 200 K to 188–190 K within 2.5 days before the observations, followed by slowly increasing temperatures during the last 12 hours as the air masses approached the Norwegian coast. As they passed over the Norwegian mountains, the air masses experienced a lee wave–generated cooling to as low as 188 K at the time of balloon encounter. Minimum temperatures were always above the ice frost point, assuming an average water vapor content of the stratosphere. Lidar observations from Kiruna and Sodankyla, Finland, limited by cloudy conditions, only occasionally showed PSC formation and layering near 22 km. A separate backscatter sonde (*14*) was launched earlier and provided some evidence for weak PSC occurrences above Kiruna. When the gondola reached a similar altitude 7 hours later, PSC activity had increased considerably. Meteorological data for that day show well-defined low-temperature regions (*13*), which proves that the measurements from the gondola were made in PSC layers controlled by lee wave activity, and not in extended PSC fields, which are common over Antarctica.

At the start of the measurements, a PSC event lasting about 8 min was encountered followed 35 min later by another PSC event lasting for 12 min when the gondola, remaining at a constant altitude, actually floated within a PSC layer. Water was monitored at mass 17 (OH^+) and 18 (H_2O^+) atomic mass units (amu) and nitric acid at 30 (NO^+) and 46 (NO_2^+) amu (fragment ions of HNO_3 are more abundant than the parent molecule of 63 amu). The spectrum was also searched for signatures of trace gases including HCl and H_2SO_4, but both were below the detection limit. Sensitivity checks after the flight showed that the lens and the analysis system performed well. The data processing included

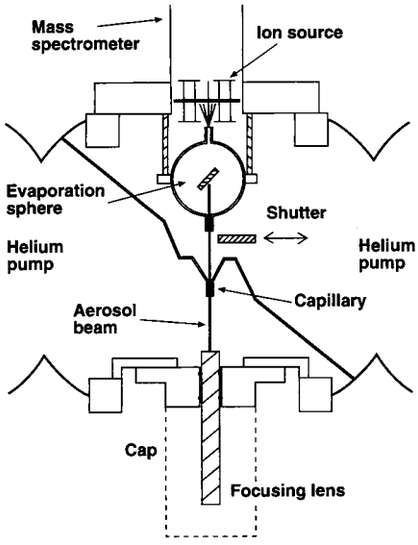

Fig. 1. Center section of the particle analysis system. An aerosol-focusing lens is located at the bottom of the gondola and is initially covered by a cap to keep the experiment under ultrahigh vacuum. When the cap is removed at the desired balloon altitude, ambient gas and aerosol particles enter the experiment through the lens in which laminar flow conditions prevail and aerosols are focused onto its axis as a narrow beam. A small hole at the exit of the lens (nozzle) determines the gas flow into the first chamber where the pressure is controlled by a liquid helium pump. The well-focused particle beam travels through a capillary into a second chamber, which contains another liquid helium pump. The particle beam finally enters a heated gold-plated sphere through a small tube and the PSC particles evaporate. A second tube points into the mass spectrometer ion source where the emerging gas molecules cross an electron beam. The resulting ions are drawn into the quadrupole spectrometer for mass separation. The right-hand liquid helium pump maintains a low-vacuum environment, particularly in the ion source region of the mass spectrometer. As a result, the system has a high sensitivity for gases released from particles.

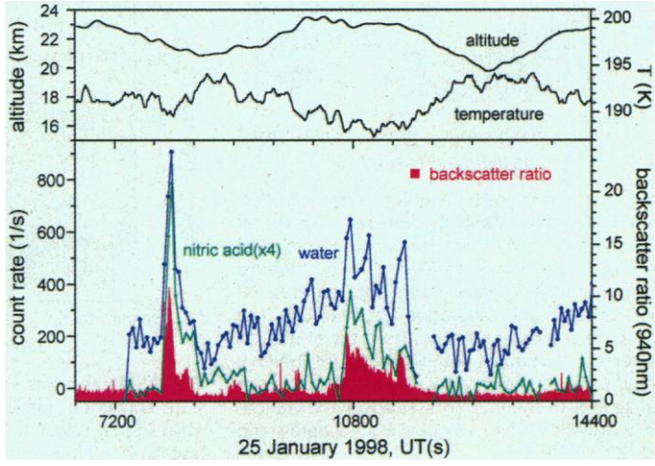

Fig. 2. Summary of data obtained during balloon flight. There are two gaps in the mass spectrometer data before 12,000 and 13,800 s when instrumental background gases were measured. Count rates at mass 18 amu are used as a measure of water and at mass 30 amu of HNO_3. Count rates for nitric acid are plotted at four times the measured value.

background corrections for the mass peaks of water and HNO_3 and the conversion of the signals to H_2O/HNO_3 molar ratios using calibration data (*16*).

A composite picture of the mass spectrometer H_2O and HNO_3 signals, the backscatter ratio, the balloon altitude, and the ambient gas temperature (Fig. 2) shows that whenever the backscatter sonde received strong signals, indicating that the gondola was within a PSC layer, both H_2O and HNO_3 signals increased rapidly. One important conclusion can be drawn immediately from Fig. 2: PSC particles do indeed contain significant amounts of H_2O and HNO_3. In the past, HNO_3 within PSC particles had only been inferred from measurements of total reactive nitrogen (*4, 17*) and from the low abundance of gaseous HNO_3 (*18*).

The temperatures have pronounced maxima and minima throughout the measurement period; the minima correlate with large backscatter and mass spectrometer signals. Together with the meteorological data this correlation supports that the measurements were made in a region controlled by mountain lee waves of estimated 10-km wavelength (*19*).

The molar ratio H_2O/HNO_3 is crucial in the characterization of PSC particles (*6*). Although the uncertainties are large, the ratios within the two PSC layers (Figs. 3 and 4) are sufficiently high to exclude NAD ($2H_2O{\cdot}HNO_3$) or NAT particle compositions, long thought to be the major nitric acid hydrates forming PSCs (*20*). Both the ambient temperatures and the ratios derived in the second layer are higher and more variable than the first (Fig. 4).

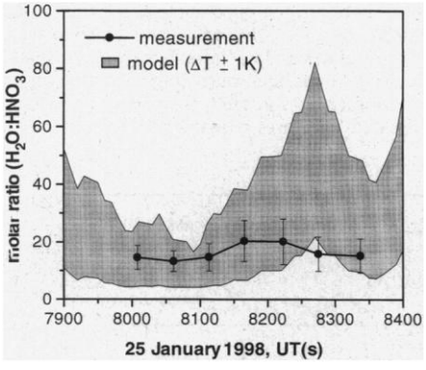

Fig. 3. Molar ratios H_2O/HNO_3 of the first PSC encounter (after 7800 s) compared with model calculations. Error bars include the statistical errors of the count rates and errors due to instrument background corrections on mass 18 and 30 amu and calibration uncertainties. The largest contribution results from the statistical error of the count rate on mass 30 (HNO_3). Model values were calculated after Carslaw *et al.* (*21*) with the following atmospheric volume mixing ratios: HNO_3, 8 ppbv; H_2O, 5 ppmv; and H_2SO_4, 0.2 ppbv.

We applied an equilibrium ternary solution model of H_2O, HNO_3, and H_2SO_4 by Carslaw *et al.* (*21*) to calculate PSC compositions using measured pressures and temperatures within a range of ±1 K and assuming an average gas phase composition for the two PSC encounters (Figs. 3 and 4). There is good agreement between the measured and the predicted ratios, which supports the interpretation that the PSCs are supercooled ternary solution particles. Model predictions are very sensitive to ambient temperatures and trace gas mixing ratios.

During the period 8500 to 10,500 s UT (Fig. 2) the temperature decreased continuously from about 194 to 190 K and the altitude changed from 21 to 23.5 km. The mass spectrometer measurements show a substantial increase in condensed water of more than a factor of 2, whereas the nitric acid signal remains near the detection limit. Although H_2SO_4 was not detected, these results can be interpreted in terms of H_2O uptake by sulfate background aerosols with decreasing temperatures (*22*). A similar effect can be observed toward the end of the flight when temperatures decreased again.

In future flights, the sensitivity of the mass spectrometer system needs to be increased to measure trace gases such as HCl dissolved in PSC aerosols. Accurate and frequent atmospheric temperature measurements are of great importance to compare the measurements with model calculations. The measurements reported here are only representative for the meteorological conditions encountered during the balloon flight. They are typical of PSCs generated in lee waves east of the Scandinavian mountains. The complexity of PSC particle formation pathways, which are a function of air mass temperatures, atmospheric trace gas concentrations, and particle composition (*22, 23*), will require additional measurements to provide broad experimental support for microphysical and atmospheric models.

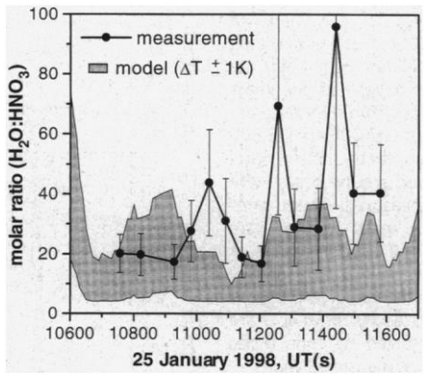

Fig. 4. Molar ratios H_2O/HNO_3 of the second PSC encounter (around 10,800 s) compared with model calculations. The same error analysis and parameters apply as in Fig. 3.

References and Notes

1. J. C. Farman, B. G. Gardiner, J. D. Shanklin, *Nature* **315**, 207 (1985).
2. P. J. Crutzen and F. Arnold, *ibid.* **324**, 651 (1986); O. B. Toon, P. Hamill, R. P. Turco, J. Pinto, *Geophys. Res. Lett.* **13**, 1284 (1986).
3. D. R Hanson and K. Mauersberger, *Geophys. Res. Lett.* **15**, 855 (1988).
4. D. W. Fahey *et al.*, *J. Geophys. Res.* **94**, 11299 (1989).
5. F. Arnold, *Ber. Bunsenges. Phys. Chem.* **96**, 339 (1992).
6. K. S. Carslaw *et al.*, *Geophys. Res. Lett.* **21**, 2479 (1994); K. S. Carslaw, T. Peter, S. L. Clegg, *Rev. Geophys.* **35**, 125 (1997); A. Tabazadeh, R. P. Turco, K. Drdla, M. Z. Jacobson, *Geophys. Res. Lett.* **21**, 1619 (1994); A. Tabazadeh and O. B. Toon, *J. Geophys. Res.* **101**, 9071 (1996).
7. T. Peter, *Science* **273**, 1352 (1996).
8. The approximate temperature range for PSC type I particles (*6*) is between 195 K, the onset of HNO_3 and H_2O uptake by background aerosols, and 188 K. Below that temperature ice particles (PSC type II) form.
9. P. Liu, P. J. Ziemann, D. B. Kittelson, P. H. McMurry, *Aerosol Sci. Technol.* **22**, 293 (1995).
10. J. Schreiner, C. Voigt, K. Mauersberger, P. McMurry, P. Ziemann, *ibid.* **29**, 50 (1998).
11. Recently, another concept in aerosol analysis was published [D. Murphy, D. S. Thomson, M. J. Mahoney, *Science* **282**, 1664 (1998)]. Laser fragmentation of single particles provides elemental composition analysis. In our experiment, a quantitative determination of the average molecular composition is made: with the present instrument sensitivity, every 50 s a H_2O/HNO_3 molar ratio is obtained.
12. The lens used for this flight focused, over a pressure range from 20 to 100 mbar, particles of radius 0.2 to 4 μm to a beam of less than 1.0 mm in diameter at a distance of 90 mm from the exit hole of the lens. The transmission efficiency is nearly 90%.
13. A. Dörnbrack, M. Leutbecher, H. Volkert, M. Wirth, *Meteorol. Appl.* **5**, 117 (1998).
14. J. M. Rosen and N. T. Kjome, *Appl. Optics* **30**, 1552 (1991).
15. Temperatures were measured 80 m above the gondola with a PT 100 sensor. Shown in Fig. 2 are temperature data averaged over 50 s and with an error of ±1 K.
16. Mass spectrometer measurements of atmospheric gases (N_2, O_2, Ar) serve as important tracers to monitor the stability of the instrument throughout the flight. Laboratory calibrations of HNO_3 and H_2O, expected to be condensed in PSC particles, were made before the flight to ensure quantitative composition analysis. Sulfate aerosols were also used to test the lens alignment as well as particle transmission and detection capability of the entire system.
17. S. R. Kawa *et al.*, *J. Geophys. Res.* **97**, 7925 (1992).
18. F. Arnold and G. Knop, *Nature* **338**, 746 (1989); H. Schlager, F. Arnold, D. Hofmann, T. Deshler, *Geophys. Res. Lett.* **17**, 1275 (1990).
19. K. S. Carslaw *et al.*, *J. Geophys. Res.* **103**, 5785 (1998); K. S. Carslaw *et al.*, *Nature* **391**, 675 (1998).
20. D. R. Worsnop, L. E. Fox, M. S. Zahniser, S. C. Wofsy, *Science* **259**, 71 (1993).
21. K. S. Carslaw, *Geophys. Res. Lett* **22**, 1877 (1995).
22. M. A. Tolbert, *Science* **264**, 527 (1994).
23. T. Koop, K. S. Carslaw, T. Peter, *Geophys. Res. Lett.* **24**, 2199 (1997).
24. Typical pressures during the balloon flight at 20 to 24 km are 10^{-3} mbar in the left chamber (Fig. 1) and 10^{-7} to 10^{-8} mbar in the right chamber. See also K. Mauersberger, *Rev. Sci. Instrum.* **48**, 1169 (1977).

25. This research was, in part, supported by the German Ozone Research program and the Commission of the European Community (N.L.). We like to thank the French and Swedish team for their impressive balloon launch and flight support. Special thanks to Jim Rosen, University of Wyoming, for letting us use his backscatter sondes. Support and information before and during the balloon flight from research groups at Andoya, Norway, Kiruna, Sweden, and Sodankyla, Finland is greatly appreciated.

16 October 1998; accepted 8 January 1999